4. Closed Loop Power Control Simulator

This chapter describes the latest and final version of the multiuser communications simulators constructed in COSSAP environment, and used to calculate the results in [P5]. In this chapter, mobile transmitter, radio channel, base station receiver, and power controller models, and their COSSAP implementations, are described in depth, also commenting on some implementation aspects arousing from COSSAP itself†. Partially similar system model concepts than simulated in this Thesis, are also described in [Cav97].

Simulators are constructed for both single user and multiuser systems, the difference of whose is evident in Section 4.4 Receiver Model. The presented single user system [P3] is of no practical value but the results serve as an introduction to the basic closed power control loop operation, which is many times is obscured in the multiuser system. The results very firmly establish the definite need for filtering in general within the closed power control loop. The multiuser simulator is an interesting system where several users, i.e., independent mobile station transmitters, are connected to a single base station. The users are individually power controlled, and interfere with each others. Adjacent cell interference and receiver noise is accounted for as added AWGN in the multiuser simulations. It would be easy to setup a multicell simulator, also. The multicell setup is described in Section 4.3 Radio Channel Model. Excluding actual system parameters, all parameters described with the respective component models are independently set for each user.

In the Figs. 4.1 - 4.3, 4.7, 4.9, 4.10, 4.12 and 4.13 below, all signal lines carry real-valued signals unless noted otherwise. A pair of signals originating from a common source and entering a common recipient forms a complex-valued signal.

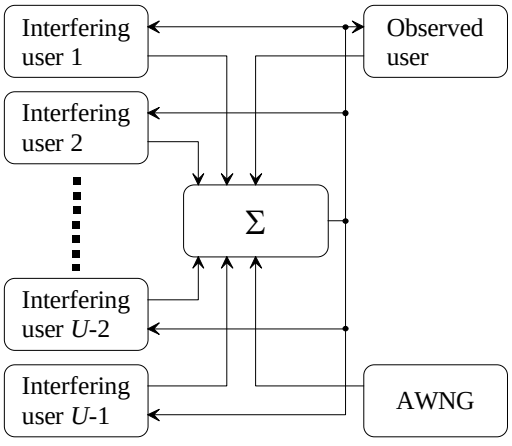

Fig. 4.1. Block diagram of a *U* user simulator. All the shown signals are complex-valued.

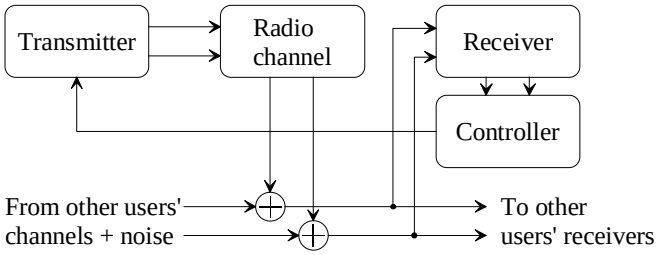

Fig. 4.2. Block diagram of a user component in Fig. 4.1. All the signals shown are real-valued.

† There exists a C-language-like number type casting feature in COSSAP, but the casting does not take the original variable type definition into account but type casting has to be done explicitly when using the parameter. The feature is that even though a COSSAP block parameter, say `$speed`, is defined to be a real number, and say, its value is a real variable divided by a constant, for example, `$speed=$mobile_speed/16`, were now the variables `$speed` and `$mobile_speed` are explicitly defined real in the design configuration, but `$mobile_speed` has an integer-like value, e.g. 10, and not 10.0, the division is carried out as integer division without type casting as expected by the design configuration variable definitions, and thus the result is truncated! The correct result is achieved for example by formatting the above parameter definition as `$speed=$mobile_speed/16.0`, which results in C-like automatic type casting. In this kind of simulation environment this can be considered a suspicious to say the least, especially as the variable definition does not cause type casting as should reasonable be expected. This feature may sometimes show up also as the reason for some unexplainable looking "divided by zero" errors when running simulations. Fortunately, none of the simulators used for *the Publications* was found to contain these truncation errors, though the "feature" was understood only at a very late stage of the research.

The overall picture of the multiuser simulator is shown in Fig. 4.1. Each user, Fig. 4.2, has its own independent transmitter, radio channel, receiver and controller components. A user transmits through his own radio channel to a common base station whose antenna sums the transmissions arriving from all the users along with some receiver noise and adjacent cell interference (the additive white Gaussian noise (AWGN) block in Fig. 4.1). The total noisy received signal is fed to each receiver, Fig. 4.2. In the multiuser simulators, after user detection, the receiver outputs the signal to the controller which makes power control decisions and sends power control command bits to the mobile transmitter accordingly.

In [P4] the chip rate is the same as in the Qualcomm system [Qua92] even though the number of chips per bit used is 127 while Qualcomm uses 128 bits per chip, whereas in [P5], the bit rate is set to 9600 bits/s, as with the Qualcomm system, resulting in a lower chip rate, while still using 127 chips per bit. Also, different seeds used in the random number generators for Rayleigh fading and AWGN generator have a little effect on the results, and thus the actual multiuser simulations give better results concerning H-N predictors in [P4] as compared to the corresponding results in [P5].

4.1 Uplink waveform

The CDMA link waveform actually used in the Qualcomm CDMA system [Qua92] is naturally somewhat more complicated than that employed in the simulations presented in this Thesis. Let us here shortly review the uplink waveform presented in [Qua92]. In that system, spreading is achieved using short pseudo noise (PN) codes of length 32768, generated with linear shift registers. The spreading code chip rate 1.2288 MHz provides for the chip rate of 128 chips per bit with data rate 9600 bits/s. Different mobile users are in turn distinguished at the base station receivers by the timing offset of a long PN sequence of length 2^{42}-1. Still, the data to be transmitted determines one of the 64 orthogonal Walsh functions which is transmitted combined with the short and long PN codes. In a multiuser CDMA system simulated in [P3], [P4] and [P5], users are detected according to the spreading codes which in the simulators are PN sequences of length 127 produced by linear shift registers. With the bit rate of 9600 bits/s, this results in the spreading rate of 1.2192 MHz employed in [P5]. In [P3] and [P4], the employed chip rate is 1.2288 MHz, and thus the bit rate is approximately 9675 bits/s.

Basis of the user detection in the presented simulators is the orthogonality of the codes, i.e., the crosscorrelations of different users' PN code sequences should be equal to zero. In the simulators described in this Thesis, interuser interference is introduced by generating the PN spreading codes of lengths 127 with shift registers with user specific initializations, since this choice for the spreading codes does not yield orthogonal codes but the correlation matrix, with the autocorrelations on the diagonal, is given by

$$XCorr = \begin{bmatrix} 127 & -1 & \cdots & -1 \\ -1 & 127 & \ddots & \vdots \\ \vdots & \ddots & \ddots & -1 \\ -1 & \cdots & -1 & 127 \end{bmatrix}. \tag{4.1}$$

In the literature, several different spreading code schemes are proposed for CDMA multiple access communications, for example [Vaj95], [Ban96], and [Lin97].

4.2 Transmitter Model

Block diagram of the mobile transmitter module, including also the transmission level setting logic, is shown in Fig. 4.3. The data to be transmitted is differentially encoded, and binary phase shift keying (BPSK) is applied [Jak74], [Car86]. Somewhat similar transmitter and receiver constructions as used in this Thesis are presented in [Cav97]. After BPSK, each BPSK block output sample is repeated for the number of chips per bit times. The sampling rate after the "Repeat for bit period" block is thus equal to chip rate. Next, the signal is spread by multiplying it with a user specific spreading code consisting of "-1"s and "1"s. Finally, transmission level is set by multiplying the signal by a power control multiplier. In the beginning of the simulation, the block "Control loop delay" produces d samples with the value $10^{-1/20}$, corresponding to the smallest possible transmission level. Subsequent transmission level settings are thus delayed by d chip periods. The total control loop delay d is realized here in order for it to effectively by the delay of the application of the power control action with respect to the channel fading. The delay d is set individually for each user, and accounts for all the loop delays, i.e., mobile and base station processing delays, and both uplink and downlink propagation delays. Also, in the beginning, a single sample with the value $10^{-1/20}$ is produced in the block "Produce on sample $10^{-1/20}$" which is multiplied by one generated by the "Produce one "1" to start loop" block, thus generating the first transmission level setting to be used in the transmission, which is repeated the number of chips per control period times to generate one sample for each transmitted chip. The transmission is thus always started using the lowest transmission power level. The production of the single samples in the beginning is necessary as COSSAP is a stream driven simulator, i.e., processing is done when all the necessary input samples are available. This means that getting the multiplicative transmission power level setting generation loop running, and also to start the overall closed power control loop, the described producing of the single samples within the loop is necessary. This also sets specific requirements for the placement of the control loop delay block. As it is the control action delay that is to be investigated, the delay has to be placed respective to the faded signal received at the base station. A COSSAP delay block generally operates so that N samples with a given value are generated before the input signal is passed through. These N samples are generated regardless of whether there are samples available in the input or not; this sample generation function is the property that actually makes it possible to get a simulator with a closed loop to run at all in a stream driven simulator like COSSAP. Placing the total loop delay block as shown in Fig. 4.3, when the simulation is started there is no power control action for the first d chip durations, and the control actions taken later are actually done based on the channel fading characteristics d chip durations in the past as desired. After the first d chip durations, for the first actual control period the transmitter power is kept at the minimum, and thereafter altered ±1 dB [Qua92] according to power control command bits received for the controller in the base station. The ±1 dB transmission level change step implies that the next transmission level setting is always generated from the last one by multiplying that with $10^{1/20}$ or $10^{-1/20}$, respectively. A single power control bit is received in the beginning of every power control period. The "Limit" block sets the dynamic range of the power control to ±15 dB from the nominal 0 dB. For the equations concerning the transmitter setup, please, cf. [P3], [P4]. In Fig. 4.3, also the different signal sampling frequencies are shown with different line types. Having three different sampling frequencies within the simulator also requires extra care for correct signal timings within the stream driven simulator.

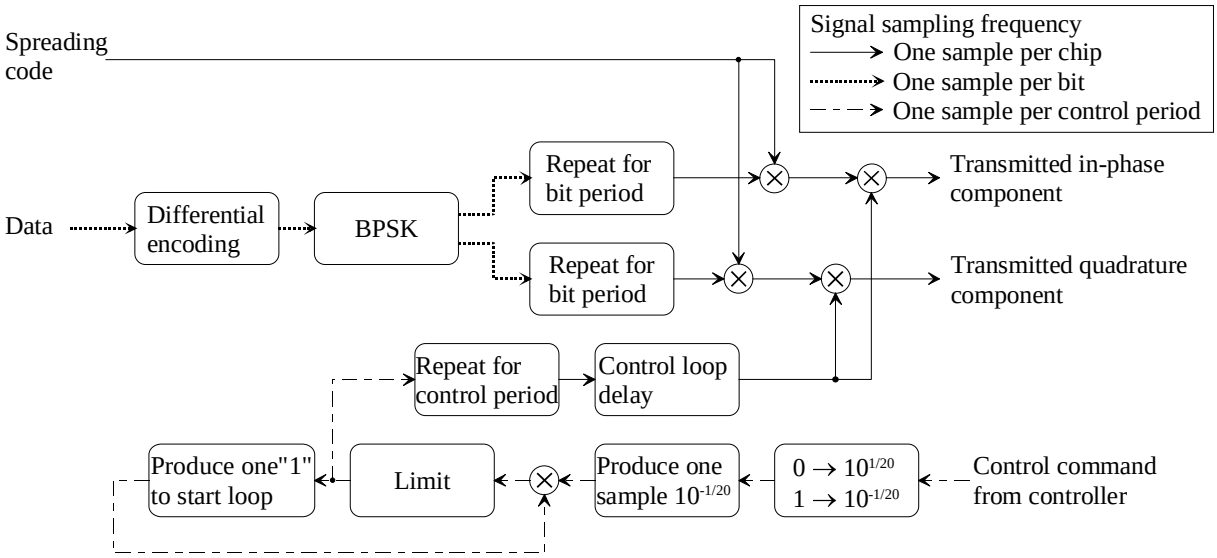

Fig. 4.3. Block diagram of the transmitter with transmitter power level setting generation. Different signal sampling frequencies are shown with different line types. The notation $X \rightarrow Y$ denotes that for each input sample with a value X, a single output sample with value Y is generated.

4.3 Radio Channel Model

Several phenomenon disturb radio transmissions in radio channels [Jak74], [Lee86], [IEE88], [Par92], [Eur93]. Distance and natural objects, like hills and forests, between a transmitter and receiver cause long term fading in the signal power. Mainly unnatural obstacles, like cars and buildings, in the radio propagation path reflect signals causing several attenuated echoes of the same transmitted signal to arrive at the receiver with different delays in different phases after traveling over different distances. This is the cause of short term fading, also called fast fading. As the mobile unit moves, the Doppler effect causes frequency shifts that may be different for each multipath component. Furthermore, the mobile speed is generally not constant, and also some of the unnatural obstacles are in constantly changing motion. These effects are illustrated in Fig. 4.4, which also illustrates the different phases of the received multipath components.

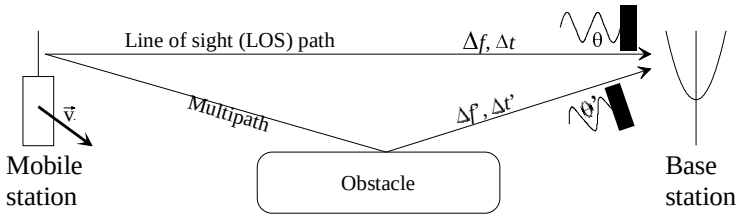

Fig. 4.4. Two multipath components arrive at the base station receiver with different Doppler frequency shifts Δf and $\Delta f'$, propagation delays Δt and $\Delta t'$, and phases θ and θ'. The mobile station is moving with the speed and direction $\vec{v}$. Also, the obstacle might not be fixed, and all the variables are generally time dependent.

Many different radio channel propagation models have been proposed to account for different channel properties. Different channel models are designed for different environments and communications systems. There exist models for rural areas, hilly terrain, urban areas, etc. [Eur93]. In general, channel properties are both frequency dependent and functions of time. The time interval over which the channel response remains approximately constant is called

the coherence time, and the frequency separation over which two signals are correlated enough is called the coherence bandwidth. The correlations to decide the coherences are to be set according to the problem at hand.

The distance between a base station and a mobile phone determines the propagation path loss in free space. This propagation path loss is only function of distance d and carrier frequency f_c [Par92], and the received-to-transmitted power ratio is given by

$$\frac{P_r}{P_t} = G_t G_r \frac{c^2}{\left(4\pi d f_c\right)^2} \tag{4.2}$$

where P_t and P_r are transmitted and received power, respectively, and c is the speed of light. G_t and G_r are the gains of transmitting and receiving antennas, respectively. The received fading signal $E(t)$, i.e., the field strength in dB in reference to a known field strength in volts/meter, is the envelope of the received radio-frequency (RF) signal. It can be modeled as being composed of a long-term fading signal $E_{long}(t)$ and of a short-term fading signal $E_{short}(t)$ [Lee86] as

$$E(t) = E_{long}(t) \cdot E_{short}(t) \,. \tag{4.3}$$

The long-term fading signal is the envelope of the received fading signal, and can be calculated from the whole fading signal as a local mean over a suitable time interval. An estimate of the local mean is given by

$$\hat{E}_{long}(t) = \frac{1}{2\Delta t} \int_{t'-\tau}^{t'+\tau} E(t)dt \tag{4.4}$$

where τ is the time interval to be chosen according to the fading characteristics. The long-term fading can also be considered to be a function of distance instead of time for path loss calculations. The problem of local mean signal strength estimation is considered in also in [Val97].

The appearances and relative amplitudes of these two fading effects depend on the environment. Fast fading is more evident in man-made environments whereas long-term fading is mostly due to landscape and line-of-sight (LOS) distances. It is not possible to define an exact frequency separating these two fadings since the long-term fading may occasionally also contain high frequency components usually encountered in fast fading signals. This happens when the non-reflected path, i.e., LOS path, is abruptly lost, for example. A radio channel with a band-limited fixed-average-power input signal, no fading, and thermal noise as the only disturbance, may be approximated by an additive white Gaussian noise (AWGN) channel [Car86]. The AWGN channel is specified as a distortionless transmission channel with a fixed bandwidth. In this model, the transmitted signal is contaminated by additive bandlimited zero mean white Gaussian noise with fixed average power. The signal and the noise used are independent so that the received signal sample is the sum of corresponding transmitted signal and noise samples, and the received average total power is the sum of average powers of the transmitted signal and the noise.

In most real environments a radio signal propagates from transmitter to receiver via many different paths, as mentioned earlier. Naturally, situations with one dominating path are possible. Different paths are caused by environmental reflectors, for example by buildings and vehicles. This multipath phenomenon causes a variety of difficulties: different paths exhibit different attenuation, the length of each path is different causing several copies of the transmitted signal to be received after different time delays with different phases and the velocity of the mobile unit to the direction of different paths is different causing each multipath component to experience different Doppler shift. When the receiving antenna sums these dispersed copies of the signal, the signal is understandably severely mutilated. In general, all these effects are time and frequency dependent, i.e., time- and frequency-selective, respectively.

Multipath propagation causes fast fading, which is also called Rayleigh fading. Assuming that the received signal consists of a large number of components with random phases, the probability density function of the signal envelope follows Rayleigh distribution that is given by

$$p(A_i) = \begin{cases} \frac{A_i}{\sigma^2} e^{-A_i^2/2\sigma^2}, & x \geq 0 \\ 0, & x < 0 \end{cases} \tag{4.5}$$

with the mean power σ^2 and short-term signal power $A_i^2/2$. Considering the signal wavelength of, for example, about 30 cm at 1 GHz, and comparing that with changes in path lengths when the transmitter is in a moving car, it can clearly be understood that the phases of the copies of the signal arriving through different paths are rapidly changing and can thus be considered random with even distribution.

In a stationary transmission setup, i.e., when neither the receiver nor the transmitter is moving and their environment is constant, the received signal is a sum of delayed copies of the transmitted signal, with a different attenuation associated with each path, given by

$$Y(t) = \sum_{i=0}^{R-1} A_i y(t - \Delta t_i) \tag{4.6}$$

where $Y(t)$ is the output of the whole channel at time t, $y(t - \Delta t_i)$ is the copy of the signal arriving through the ith path with delay Δt_i, A_i is the attenuation associated with the ith path and R is the total number of paths. If the system is not stationary, amplitude coefficients, delays and the number of paths may be time varying. Even if the system is completely stationary the copies of the signal reach the receiver in different phases according to the lengths of the paths. Given the length difference of two paths as $\Delta l(t)$, the phase difference is given by

$$\Delta\theta(t) = 2\pi\Delta l(t)/\lambda \tag{4.7}$$

where λ is the wavelength. In addition, if the mobile unit is in motion the transmitted frequency suffers from a Doppler shift

$$\Delta f(t) = v\cos\alpha(t)/\lambda \tag{4.8}$$

where v is the speed of the mobile unit and $\alpha(t)$ is the angle between the direction of the mobile speed and the transmitted wave. From (4.8) it can be seen that the maximum increase in frequency is encountered while the mobile is moving directly towards the base station and the maximum decrease while moving straight away from the base station. In (4.7) and (4.8) the original transmitted frequency and the speed of the mobile are considered constant, but in practice they may be time dependent as well.

Including all these effects and considering R resolvable multipath components, each composed of M waves with possibly different delays Δt_{nm} arriving at the receiver with equal Doppler shifts f_{Dn}, the received signal can be modeled as [Jak74]

$$E(\omega,t) = E_0 \sum_{n=1}^{R} \sum_{m=1}^{M} A_{nm} \cos\left(f_c t + f_{Dn} t - f_c \Delta t_{nm} \right). \tag{4.9}$$

Differing delays cause phase distortion $f_c \Delta t_{nm}$ of the signal. The original transmitted frequency is f_c, and E_0 is the amplitude of the transmitted signal. Coefficients A_{nm} reflect different signal power attenuation associated with each wave. In all practical cases each parameter in (4.9) is, at least in principle, time dependent. Effects of multipath on CDMA cellular communications are analyzed in [JaH94] and [Cha94], and estimation of propagation delays Δt is considered in [Str96].

Naturally, the channel simulator should produce as realistic power responses as possible. Minimum model input parameters are the mobile speed and carrier frequency, or the input signal envelope, or the actual transmitted waveform. It would also be of interest that the model could produce different channel responses according to the environment type, like urban area, given as an input. Predictors could also be designed using real measurement data but the resulting predictor would probably be too environment specific with no capabilities to function under a wider range of conditions but only in the conditions close to those of the measurements used.

In this work, the channel model employed is a single Rayleigh fading propagation path contaminated by additive white Gaussian noise (AWGN), and it is presented in the base-band. Now in (4.9) $R = 1$, and A_0 is Rayleigh distributed with AWGN added independently to the quadrature components. The AWGN presents receiver noise. The assumption on Rayleigh distributed received signal power is valid on a narrow-band communications systems, but not generally in CDMA systems. A CDMA the radio channel model consisting of a single Rayleigh fader would be overly pessimistic since because of the wide transmission band the fading cannot be considered frequency flat, i.e., the fading is frequency depended. Thus, some power is always available at some portion of the wide transmission band. A RAKE receiver [Pri58] is capable of distinguishing between different paths with sufficient delay separation. Implicitly including a good enough RAKE receiver within the radio channel model results in a single Rayleigh fader channel model to be seen through a single RAKE finger. Within the work presented here, RAKEs are not explicitly employed because the intention is to clearly see the effects of applied predictive filtering, and multipath combining, even though it would give better BER results in the simulation, would very probably obscure the results at least to some extent. Also, employing RAKEs would also mean employing actual multipath radio channel models into the simulations. But, as mentioned, the single Rayleigh fader channel model assumption can be considered to implicitly include a RAKE receiver. Performance of

RAKE receivers with random spreading sequences is analyzed by Cheun in [Che97], and a decision-directed SS RAKE is presented in [Pov96].

4.3.1 Jakes' Rayleigh Fader

In [P2] the Jakes' Rayleigh approximation [Jak74] is employed. In the Jakes' Rayleigh fader the Rayleigh distributed signal is approximated by sums of appropriately chosen sinusoids whose frequencies correspond to the Doppler shift frequencies [Jak74]. Jakes' Rayleigh fading model is further improved in [Den93].

4.3.2 Noise Shaping Rayleigh Fader

One other way to generate a signal whose amplitude distribution follows Rayleigh distribution is by summing two independent squared zero mean white Gaussian (WGN) noise processes [Car86]. The noise shaping Rayleigh fader, with also signal power calculation shown, is illustrated in Fig. 4.5. Since only the baseband equivalent signals are considered, the carrier mixer is not shown. The subscript "*i*" denotes the real part, i.e., the in-phase component, and the subscript "*q*" the imaginary, i.e., the quadrature component of the complex-valued baseband equivalent signal, and "$(\ )^2$" denotes squaring operation. The baseband equivalent signal components are formed by filtering two independent WGN processes by two identical but separate noise shaping filters (NSF) which are chosen according to the antenna geometry selected to be analyzed [Gan72]. The shaped noise sequences are then squared and summed to produce the Rayleigh fading signal power. Receiver noise and adjacent cell interference are simulated by adding zero mean additive white Gaussian noise (AWGN) to the in-phase and quadrature components independently before the squaring operation. In the simulations, the NSF approximates the received spectrum $S(f)$ given theoretically by [Jak74] as

$$S(f) = \frac{1}{\sqrt{1-\left(\frac{f-f_c}{f_{D\max}}\right)^2}}, \tag{4.10}$$

where f is frequency, f_c is carrier frequency and $f_{D\max}$ is the maximum Doppler shift frequency. The relations between spectra and antenna geometries are analyzed in [Gan72]. In [P1], the maximum Doppler shift frequency is derived from the vehicle speed which is set to either 5 km/h or 50 km/h, corresponding to the slow and high urban speeds, respectively, and the carrier frequency is set to 1800 MHz. As any filter with frequency response corresponding to the power spectrum of the antenna is suitable as the NSF, a 4000 tap FIR was designed to provide a good enough approximation of the desired frequency response [P1]. It was verified that the frequency responses closely matched the corresponding theoretical spectra for a vertical omnidirectional antenna. Before demodulation the spectrum is centered at the carrier frequency. At demodulation it is shifted to baseband, and centered at zero frequency.

In the standard COSSAP Rayleigh fader block, a fixed narrow-band lowpass NSF ("Spectrum shaping IIR" in Fig. 4.7) is used, and an interpolator takes care of the mobile speed and carrier frequency settings. In the original COSSAP Rayleigh fader model, two interpolators are used to achieve the correct interpolation ratio with the GSM system parameters. With the system

parameters applied here, a single interpolator is sufficient, though. The COSSAP NSF frequency response along with the theoretical response for an omnidirectional monopole antenna [Gan72], [Jak74] (4.10) is shown in Fig. 4.6. The NSF cutoff frequency, 0.00904956 in normalized frequency scale, and the NSF gain along with the set variance of the source WGN, are set so that the average power of the fader output signal can be set by simple multiplication by the desired average power setting, Fig. 4.7.

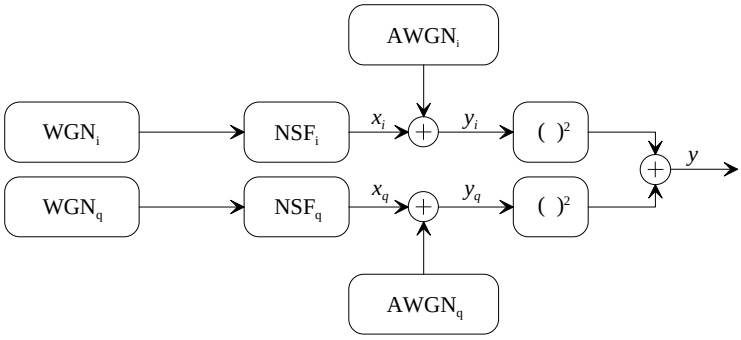

Fig. 4.5. Noise shaping Rayleigh fader. WGN is a white Gaussian noise process, AWGN is an additive WGN and NSF is a noise shaping filter.

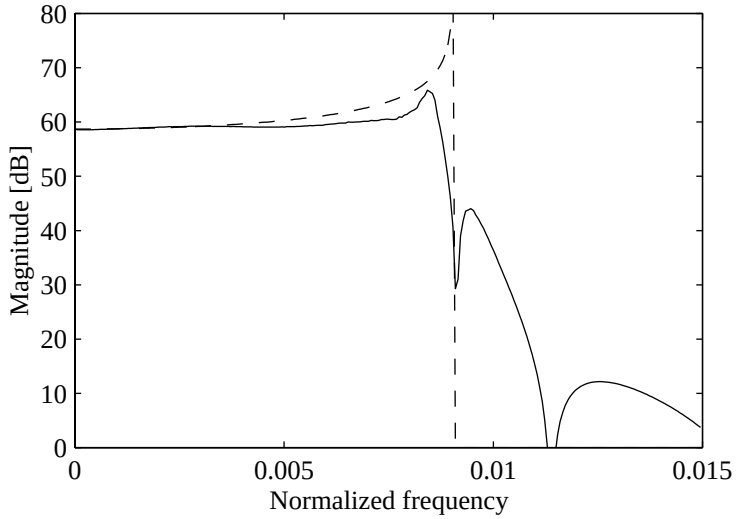

Fig. 4.6. Frequency response of the COSSAP Rayleigh fader IIR NSF (solid) along with the corresponding theoretical response (4.10). The theoretical response is scaled to have DC gain equal to that of the COSSAP NSF.

The radio channel model used in the simulations [P3], [P4], [P5], Fig. 4.7, is a single tap Rayleigh fading channel model in which Rayleigh fading is generated by noise shaping. First, a complex white Gaussian noise (WGN) signal is generated. The spectrum of the noise is shaped by a noise shaping filter. The filter is a standard COSSAP block and is selected so that the resulting noise spectrum corresponds to that seen by a single omnidirectional monopole antenna at the base station receiver. The passband width of the filter is set so that the final fading bandwidth, determined by the carrier frequency and mobile speed, can be set by interpolating the signal. After spectral shaping, the average fading signal power is set, and some first samples are deleted in order to allow for the noise shaping filter to settle. Finally, linear interpolation is applied to yield a correct fading signal bandwidth, and the fading is

applied to the transmitted signal. The output fading power of the Rayleigh fader in Fig. 4.7, is illustrated in Fig. 4.8.

Each mobile has a fading channel of its own, and the mobiles interfere with each other also through these same channels. This corresponds to the case where all the mobiles are connected to the same single base station. This single cell system can easily be changed to a multicell setup by introducing one radio channel per user per cell for adjacent cell interference, in addition to the different channel for intracell interference and transmission.

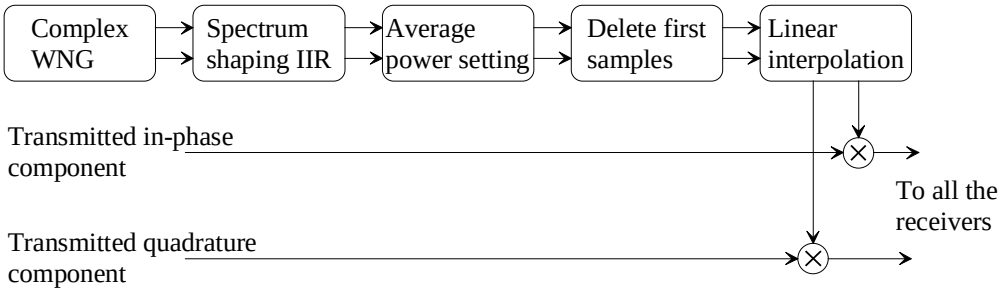

Fig. 4.7. Block diagram of the Rayleigh fading channel model.

The main difference between the Jakes' and the noise shaping Rayleigh faders is the frequency distribution. In the Jakes' fader, there is a number of distinct frequency components, carrying also all the signal power. On the other hand, in the noise shaping fader, the signal power is theoretically continuously distributed. Filtering the fading signal with a lowpass filter whose passband edge is close to the fading signal bandwidth, naturally distorts the signal, and in the case of the Jakes' fader, the distortion close to the maximum Doppler frequency frequency component may have a major effect on the power contained within the fading signal. With the noise shaping fader, this effect is not as severe.

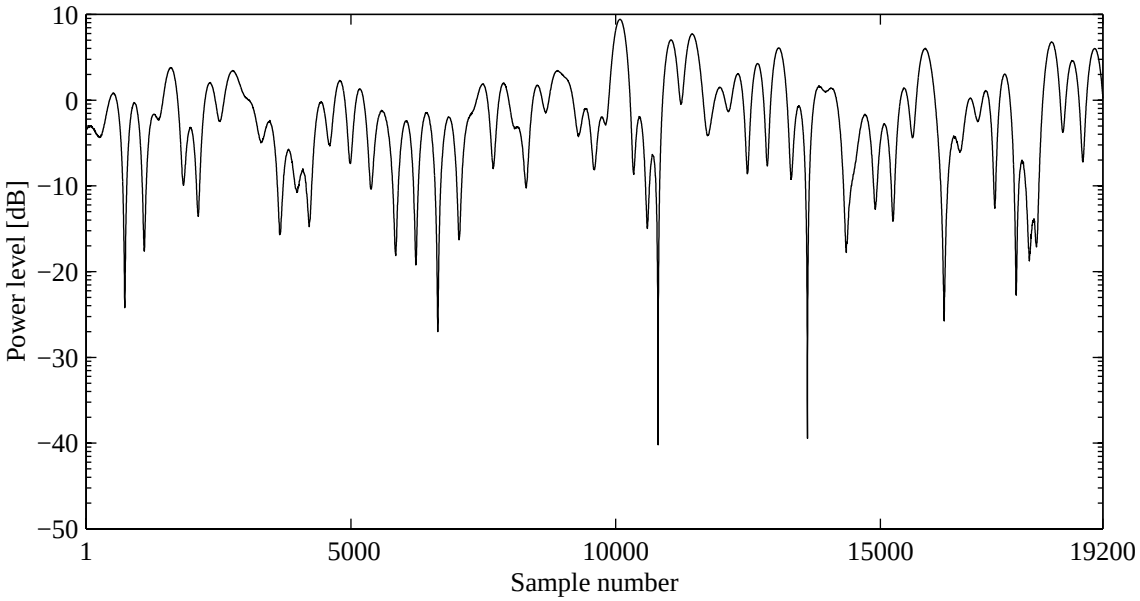

Fig. 4.8. Two seconds of the power of the Rayleigh fader output, i.e., the sum of squares of the "Linear interpolation" block outputs in Fig. 4.7, at mobile speed of 10 km/h, carrier frequency 1.8 GHz, and with the average fading power set to 0 dB, sampled at 9600 samples/s.

4.4 Receiver Model

For these simulators, the single user and multiuser receiver [Car86], [Gib96] models, Figs. 4.9 and 4.10, respectively, turn out to be very simple. Somewhat similar transmitter and receiver constructions as used in this Thesis are presented in [Cav97]. The received total complex-valued signal, consisting now of the transmissions from all the users and some AWGN, is despread by multiplying it with the desired user's spreading code. Here it is assumed that the spreading codes are known and precisely synchronized. The despread signal is integrated over the bit duration to yield an estimate of the accumulated signal energy from the desired user. This is also the signal that is fed to the controller as input in the multiuser simulators. In the single user simulators, the input to the controller is the despread signal which is only decimated to yield a sampling rate equal to the bit rate. For clarity, the decimator is here shown within Fig. 4.9, even though in the simulator it resides within the controller block. The integrated signal is then BPSK demodulated. The COSSAP BPSK block also makes the bit decisions based on the Euclidean distances from the received complex signal samples to the constellation points. In the bit-error-rate (BER) calculation, the received signal is compared with the actual transmitted data.

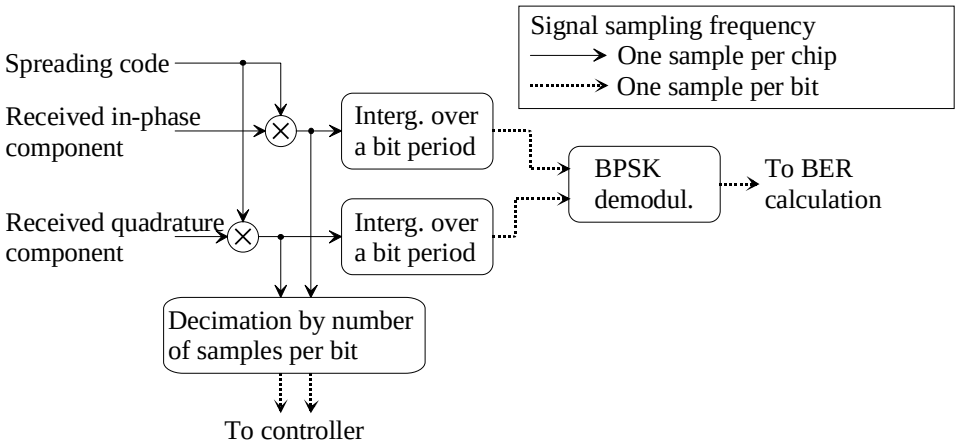

Fig. 4.9. Singleuser simulator receiver block diagram. In the simulator, the decimator resides within the controller but is shown here for the clarity.

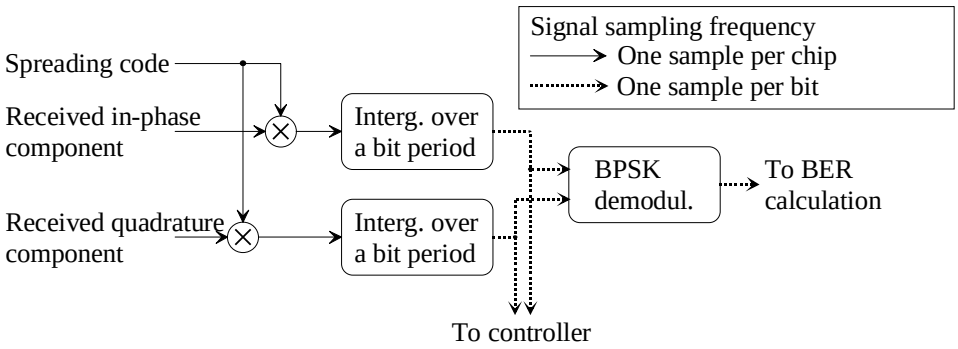

Fig. 4.10. Multiuser simulator receiver block diagram.

4.5 Power Controller Model

Increasing the capacity of a DS/CDMA system by improving the uplink power control system [Cha96], [Qua92] functionality is the motivation of the work presented in this Thesis, although predictive filtering in general is a powerful tool for variety of applications. It has been widely studied in the literature that the user capacity of a CDMA network is crucially dependent on the effectiveness of the power control system [Gil91], [Vit93b], [Ari], [Lee97], [Ada96]. This is because the system capacity is interference limited, and it is thus of great importance that all the mobile users are received at the base station at an equal constant power level. Also, the transmitter power of each mobile is to be kept as low as possible to reduce interference and save batteries. A closed power control loop is illustrated in Fig. 4.11.

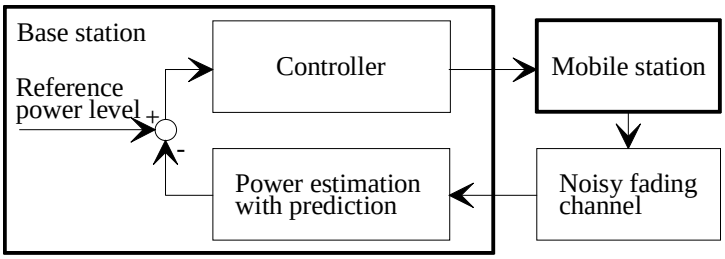

Fig. 4.11. A closed power control loop in a CDMA system.

A general reference to adaptive feedback, i.e., closed loop, control is [Åst87], and signal and interferences statistics for CDMA systems with closed loop power control are discussed in [Ari]. A CDMA system employs transmitter power control on both uplink [Qua92], [Cha96] and downlink [Qua92], [Lee95] direction. Only uplink power control functions are considered in this Thesis. In the downlink, it is generally possible to synchronize the transmissions and thus have better cross correlation properties between the CDMA codes at the mobile receiver. In the uplink this synchronization is not possible, or at least it is very difficult to realize.

4.5.1 The Qualcomm System Downlink Power Control

The uplink power control in the Qualcomm CDMA system [Qua92] includes both closed and open power control loops. The functioning of the open loop is based on the measurements made by the mobile station itself of the downlink channel, and therefore the measurement results are available for quick application. The open loop power control is used in situations where it is desirable to quickly reduce the transmitter power, as is the case, for example, when the mobile moves around a corner and a LOS path suddenly becomes available. This reduces unnecessary interference that would be caused otherwise. On the other hand, as the measurements are done from the downlink channel, and as the frequency separation between uplink and downlink channels, 45 MHz, exceeds the coherence bandwidth, the Rayleigh fadings are independent in the two channels, and thus the open loop power control cannot be used to fight the Rayleigh fading. The open loop control is also allowed to increase the transmitter power but the rate of increase is generally limited to the rate that the closed loop power control is able to compensate to avoid unnecessary interference in the case that the open loop decision had been wrong. The closed loop power control is based on the measurements done by the base station of the uplink channel. The base station sends power control commands to the mobile stations according to measured SNR, and the mobile station adjusts its transmitter power combining both open loop decisions and closed loop commands.

The open loop power control operation tries to maintain the power level received from all the mobile station on a constant nominal level and has dynamic range of about 85 dB or more. The closed loop power control response time is obviously slower than that of the open loop, but as the measurements are done in the uplink channel itself, the measurements show the actual Rayleigh fading in the channel and thus the closed loop power control is used to fight the Rayleigh fading. It is well understandable that in the this kind of closed loop control, latency minimization is of great importance as the channel should have remained essentially unchanged during the latency for the control to be effective. In the Qualcomm CDMA system, the power control commands are sent every 12 bits, i.e, every 1.25 ms, and the effect of each closed loop power control command to the mobile transmitter power is approximately ±0.5 dB.

4.5.2 Power Control in the Simulator

Power controller model block diagrams for single user and multiuser simulators are shown in Figs. 4.12 and 4.13, respectively. The input to the controller in the multiuser simulators is a signal which is already despread and integrated over the bit duration in the receiver. It is to be noted that the integration in the receiver readily removes much of the noise present in the received signal. The effect of this phenomenon is discussed in conjunction with the simulation result analysis.

The control is based on the estimated received signal power level originated from the mobile being controlled. The aim of the power control is to maintain the desired received power level irrespective of the fading and interference. It is assumed that the power control and data modulations of the received signal can be completely removed in order to obtain a predictable radio channel estimate which is then scaled by the number of chips per bit. It is assumed that in a real case, error correction coding [Qua92], [Vit95], [Gib96] and other means of improving BER would be used, and the system could provide low enough BER so that the phase error would be infrequent enough not to affect the controller performance too much. Here, as no error correcting coding is employed, i.e., the system produces so called raw BERs, there would be too many errors in the received data in order to do the data removal according to the actual received data, and thus ideal data modulation removal is assumed, and also transmitter power level setting is always known by the base station. The prediction is independently applied to the in-phase and quadrature components of this estimate. After prediction, the transmitter power level information is restored by multiplying the predicted chip components with the corresponding transmitter power level setting. Signal power estimate is calculated by computing the sum of squared in-phase and quadrature components, the power estimate is integrated over the control period in bits, and scaled by the number of bits in a control period. This presents the predictive estimate $\hat{P}_r$ (4.11) of the received average signal power originating from the particular user's mobile transmitter. The scalings are performed in order to be able to set the desired signal threshold level to unity, i.e., to 0 dB.

$$\hat{P}_r(n_c) = \frac{1}{M}\sum_{m=1}^{M}\left[c(n)\sum_{k=1}^{K} h(k)\frac{x_i(n-k)}{c(n-k)} + c(n)\sum_{k=1}^{K} h(k)\frac{x_q(n-k)}{c(n-k)} \right]^2, \qquad (4.11)$$

where n is the bit time index,
n_c the control command time index, sampled at the same time with every Mth n,

M the number of bits per control interval,
$c(n)$ the transmitter power level setting,
K the number of FIR coefficients,
$h(k)$ the coefficients of the predictive finite impulse response filter, and
x_i and x_q the in-phase and quadrature components of the controller input,
respectively, from which the power control and data modulations have been removed. The reference controllers are exactly identical with the corresponding predictive controllers, except that the predictors are omitted.

Finally, the power control bit to be sent to the mobile transmitter is generated using a threshold function, so that if the input to the thresholder is larger than 1 a control bit "1" is output to reduce the transmitter power, and correspondingly if the input to the thresholder is less than 1 a control bit "0" is output to command for increase in the mobile transmitter power level. The power controller setpoint is thus 0 dB. Possible power control bit transmission errors are not accounted for in the simulator.

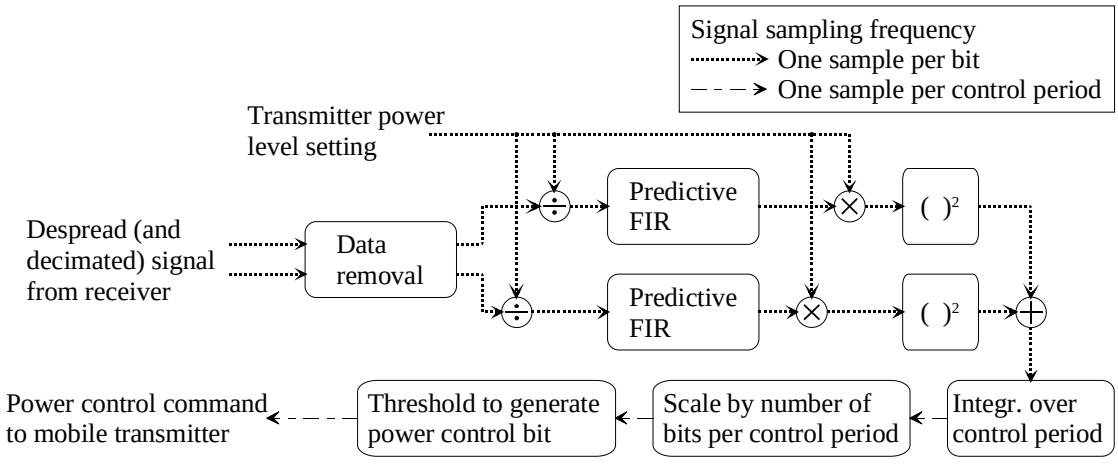

Fig. 4.12. Block diagram of the predictive singleuser power controller. Prediction is done in components at bit rate. In blocks with two input and two output signals, the processing is done independently to the upper and lower input signals. In the actual simulator, decimation of the input is done in the controller block.

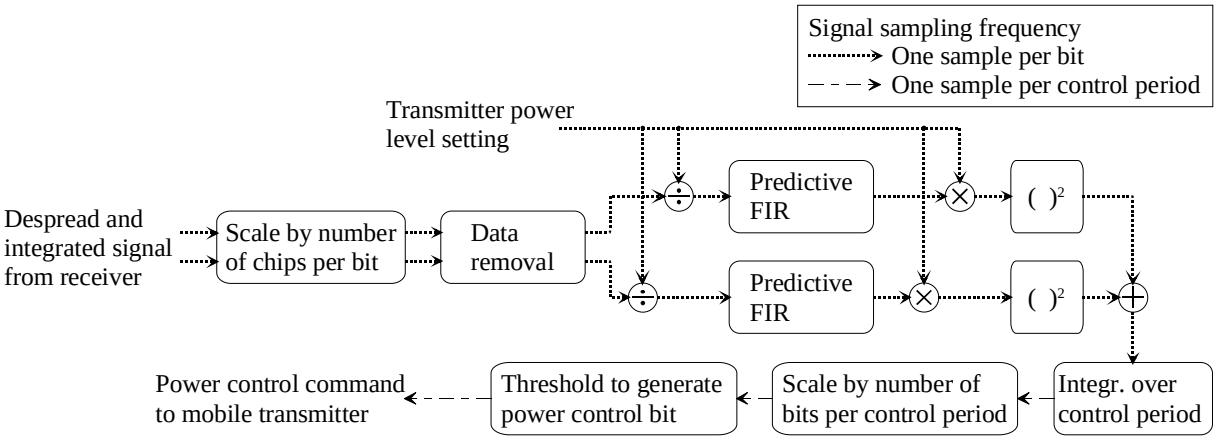

Fig. 4.13. Block diagram of the predictive multiuser power controller. Prediction is done in components at bit rate. In blocks with two input and two output signals, the processing is done independently to the upper and lower input signals.

For the control equations, please cf. [P3], [P5], and Chapter 8 Errata of *the Publications*.